Metals and Materials International
https://doi.org/10.1007/s12540-022-01356-9

# Productivity Enhancement in Directed Energy Deposition: The Oscillating Scanning Strategy Approach

**Alberta Aversa[1,2] · Alessandro Carrozza[2,3] · Giulio Marchese[1,2] · Stefano Felicioni[1] · Michele De Chirico[4] · Mariangela Lombardi[1,2] · Federica Bondioli[1,2] · Paolo Fino[1,2]**

Received: 11 October 2022 / Accepted: 24 November 2022


**Abstract**
Directed Energy Deposition (DED) is an additive manufacturing process that enables the production of large metal components by melting the feedstock material while being deposited. An improvement of the production speed of this process would further increase its applicability in many industrial fields. The DED building rate is strictly related to the building parameters adopted, in particular to the laser spot diameter, which also affects the build accuracy and the surface quality of the components. The possibility of using a variable laser spot would result in a significant increase in the production rate in bulky zones, while also providing a good surface quality where needed. In the present work, an oscillating scanning strategy was used to create a large apparent laser spot (+ 170% of the nominal value) to produce 316L stainless steel samples via DED. The optimisation of the DED parameters with the oscillating strategy was performed using the single scan tracks (SSTs) approach. The morphologies of the SSTs obtained with different process parameters were assessed and the geometrical features related to the melt pools were analysed in order to select the most suitable X and Z displacements for the production of the cubic samples. The analyses of the cubes revealed that, if the correct overlap among nearby scans is selected, it is possible to obtain dense samples with all the oscillating diameters tested. Finally, comparing the building rate and powder efficiency values confirmed that this method can accelerate the building process and improve its overall performance.

**Keywords** Additive manufacturing · Directed energy deposition · Steel · Oscillating strategy · Laser · Building rate

## 1 Introduction

It is well established that the improvement of the building rate is one of the crucial technical aspects faced by Additive Manufacturing (AM) research activities. An increase in productivity would make AM technologies more suitable and attractive for several industrial fields.

Directed Energy Deposition (DED) is one of the most promising AM technologies in terms of building rate. The DED process enables the production of metal components via in-situ delivery and melting of the feedstock material, either in the form of powder or wire. The success of this AM process is not only due to its high building rate but also to the possibility of repairing/rebuilding parts and the ability of producing large and functionally graded components.

The selection of the optimum DED parameters such as laser power, scanning speed, laser spot, dX and dZ is fundamental to produce fully dense parts. In particular, the consolidation of components during DED is related to the size and the geometry of the melt-pool and to the interaction between nearby ones. These features are a consequence of the interaction among all the process parameters [1]. Because of these reasons, to avoid defects such as spattering, porosities or inclusions, these interactions must be carefully considered. Moreover, the DED building parameters also affect the material thermal history and consequently the part microstructure and properties. It is well known that large thermal gradients

✉ Alberta Aversa
alberta.aversa@polito.it

[1] Department of Applied Science and Technology, Politecnico di Torino, Corso Duca Degli Abruzzi 24, 10129 Turin, Italy

[2] Consorzio Interuniversitario Nazionale per la Scienza e Tecnologia dei Materiali (INSTM), Via G. Giusti 9, 50121 Florence, Italy

[3] Department of Engineering and Applied Science, University of Bergamo, Viale Marconi 5, 24044 Dalmine, BG, Italy

[4] Prima Industrie S.P.A, Via Torino Pianezza 36, 10093 Collegno, Italy

Published online: 31 December 2022

typical of the DED process are able to generate a very fine microstructure. The size and the geometry of the microstructural features can be influenced by the thermal gradient values and modified by varying the scanning speed and using differently localized energy sources [2].

As reported by Francis, the DED building rate is strongly influenced by the process parameters, particularly by the laser spot size [3]. Mudge and Wald reported that a larger laser spot in a DED system grants higher deposition rates and powder efficiencies [4, 5]. However, it was also demonstrated that higher surface roughness and lower geometrical accuracy are generally obtained when large laser spots are used. When a DED part requires finishing, the surface quality may not be relevant and hence a large spot can be used. Nonetheless, when the part has to be used in the as-built state, achieving a smooth surface and good geometrical accuracy is important, hence low spot sizes are generally preferred at the expenses of the deposition rate [6]. For the DED production of these parts, a variable laser spot size would allow to maintain a high quality of the surface when needed and a high building rate in the bulky areas (e.g. core).

The idea of a variable spot size in AM was already suggested in 1997 by Miller et al. [7]. The laser spot of most AM systems is, however, fixed at a certain focus distance, thus being hardly adjustable during the building process. In order to overcome this limitation, Miller et al. built steel samples using a modified Selective Laser Sintering (SLS) system characterized by four spot sizes [7]. Later, Yi et al. used a dynamic focus mirror to dynamically change the focus distance, hence the spot size, of a UV laser beam of a stereolithography system [8].

Another promising way to rapidly modify the melt pool size is to use an oscillating laser scanning strategy. This method, which is known in welding as wobbling, creates an apparent laser spot larger than the nominal one by oscillating the laser using specific patterns, amplitudes and frequencies. As reported in the literature the advantages of the oscillating scanning strategy in welding are related to the possibility of changing the laser spot and also to the reduction of the hardness of the heat-affected zone, the brittle phases content and the melt pool emission (e.g. spatters) [9–11]. Ramiarison et al. used this strategy to weld Al alloys and demonstrated that these effects are obtained by increasing the melt pool area, thus reducing its cooling rate [12]. Furthermore, Hagenlocher et al. demonstrated that the modification of the solidification conditions also has a strong influence on the microstructure of the solidified weld pools [13]. Therefore, this method has been widely used to weld critical metals such as copper, structural steels or dissimilar materials characterized by different thermo-physical properties [3, 10, 11]. To the best of the authors' knowledge, this method has never been used in the metal AM field [14].

In this work an oscillating strategy was used to process a AISI 316L stainless steel powder by means of DED with the aim of tailoring its productivity. The effects of the oscillating parameters on the melt pool geometry, densification, building rate, powder efficiency, microstructure and surface quality were analysed.

## 2 Materials and Methods

A 316L gas-atomised powder with a particles size in the range 50-150 μm was used to produce all the samples. The DED system deployed is a prototype produced by Prima Additive S.p.A. composed of a 3-axis CNC unit [15].

The main process parameters of the DED process with the oscillating strategy are the powder feed rate (F), the laser power (P), the scanning speed ($v_S$), the laser spot ($d_F$), the oscillating diameter ($d_o$) and the oscillating frequency ($f_s$). A schematic representation of the laser pattern is reported in Fig. 1.

In the first experimental step, 30 mm-long single scan tracks (SSTs) were built with different combinations of process parameters. Due to the large number of process and oscillating parameters introduced by the oscillating strategy, some of them were kept constant and selected based on the authors' knowledge. The nominal laser spot, $d_F$, was 2 mm, the powder feed rate, F, was kept constant and equal to 15 g/min and $f_s$, the oscillating frequency, was set as 250 Hz. The laser power and the scan speed were varied in ranges selected to provide an energy density (ED) value close to the value used in previous works (75 J/mm$^2$) by Aversa et al.[16].

The ED was evaluated as:

$$ED = \frac{P}{v_s \cdot d_F} \tag{1}$$

The building parameters used to deposit SSTs are reported in Table 1.

These parameters were selected to provide an oscillating overlap ($OV_{OSC}$) higher than 90 %. The $OV_{OSC}$ represents the degree of overlap among consecutive circles (See Fig. 1) and can be calculated as reported by Franco et al. [17]:

$$OV_{OSC} = \frac{X_1}{X_2} * 100 = \frac{\sqrt{4A^2 - \left(\frac{v_s}{\pi f_s}\right)^2} - \left(\frac{v_s}{2\pi f_s}\right) * \left(3\pi + 2\arcsin\left(-\frac{v_s}{2\pi f_s A}\right)\right)}{\sqrt{4A^2 - \left(\frac{v_s}{\pi f_s}\right)^2} - \left(\frac{v_s}{2\pi f_s}\right) * \left(\pi + 2\arcsin\left(-\frac{v_s}{2\pi f_s A}\right)\right)} \tag{2}$$

These $OV_{OSC}$ values were selected because, as reported by Franco et al. [17], the oscillating overlap has a strong effect on the melting mode. Low overlap values cause the formation of deep melt pools in the keyhole melting mode, while high overlaps cause the formation of conduction mode pools. The keyhole melting mode arises when the melt pool temperature reaches the metal boiling point; therefore, a recoil pressure is generated, resulting in extremely deep melt pools. This melting mode is strongly undesired in AM, as it requires high energy consumptions. Moreover, it might cause the modification of the alloy's composition and the formation of keyhole pores. Because of this reason all the AM process optimisations aim at obtaining the conduction melting mode which causes the formation of more appropriate melt pool shapes.

All SSTs were at first analysed by means of on-top imaging using a Leica EZ4 W stereomicroscope. Afterwards, all the samples were cut in their centre perpendicularly to the scanning direction, mounted, ground and polished down to 0.03 µm in order to analyse the melt pool's geometries, using a LEICA DMI 5000 M optical microscope. The software ImageJ was used to analyse the main geometrical features of the melt pools: growth (G) and width (W), as schematized in Fig. 2.

In a second experimental step, 20 mm x 20 mm x 20 mm cubes were built with some of the SSTs parameters sets (P=1500 W, $v_s$= 600 mm/min and all $d_o$ values) using 20, 30 and 40% X overlap ($OV_X$) and 10% Z overlap ($OV_Z$). These overlap values, reported in Table 2, were selected based on the author's previous work on the same material [16]. The X and Z displacements (dX and dZ) were calculated as:

$$dX = W \cdot \left(1 - OV_X\right) \tag{3}$$

$$dZ = G \cdot (1 - OV_Z) \tag{4}$$

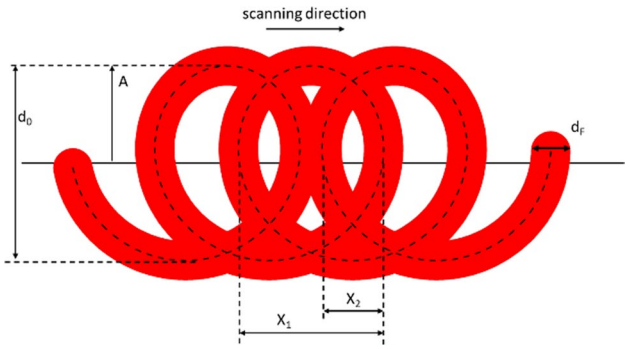


**Fig. 1** Schematic representation of the laser pattern with the oscillating strategy. $d_o$ is oscillating diameter, $d_F$ is the nominal laser spot, A is the oscillating amplitude, $x_1$ and $x_2$ indicate the overlapping length of consequent oscillations

**Table 1** SSTs DED parameters

| P (W) | $v_s$ (mm/min) | ED (J/ mm$^2$) | $d_o$ (mm) |
|---|---|---|---|
| 1000 | 400 | 75 | 0 |
| 1500 | 600 | | 0.9 |
| 2000 | 800 | | 1.7 |
| 2500 | 1000 | | 2.6 |
| | | | 3.4 |

The deposited cubes were measured using a calliper. The dimensions of the cubes were evaluated as mean value of three measurements taken at different locations. These values were then used to evaluate the deposited volume ($V_d$) and to calculate the building rate (BR) and powder efficiency (η), as:

$$BR = \frac{V_d}{t_d} \tag{5}$$

$$\eta(\%) = \frac{F \cdot \left(\frac{V_{th}}{BR}\right)}{V_d \cdot \rho} \tag{6}$$

where $V_{th}$ is the theoretical volume, $t_d$ is the deposition time and ρ is the material density.

The cubes were cut in their centre, mounted, ground, polished down to 0.03 µm and observed by means of optical microscopy. The porosity content was evaluated by image analyses, using the ImageJ software. Finally, the cubes were etched with a Kalling's No. 2 solution for 10 s to assess the effect that the oscillating strategy had on the material's microstructure. The Primary Dendrite Arm Spacing (PDAS) values of the samples were evaluated by image analyses using the images J software. Per each sample, 15 images taken at different height were analysed.

The mechanical behaviour of the parts was evaluated by Vickers hardness tests. Five measurements were performed on the samples Z cross-section using 300 g and 15 s.

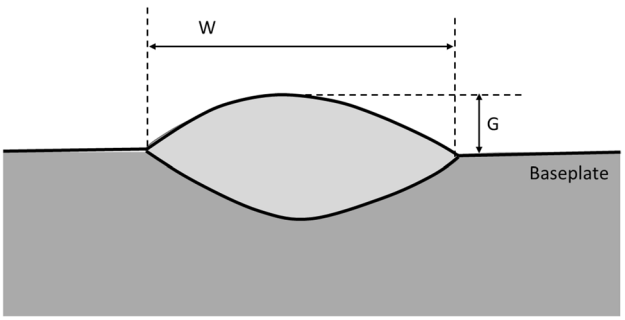


**Fig. 2** Geometrical features of the SSTs melt pools. G and W respectively indicate the growth and the width of a melt pool

The surface quality of the lateral surfaces of some samples was measured by means of confocal imaging, deploying a Sensofar S Neox 3D optical profilometer. The Sa and Sz parameters were evaluated to compare the different surfaces, according to ISO 25178. A 10x magnification lens was used to investigate an area ranging from 17.5 mm x 16.2 mm to 18.9 mm x 18.9 mm. The surface reconstruction maps were investigated using the Mountains Maps Premium 7.4 software.

## 3 Results and Discussion

At first, the on-top observations of the tracks revealed the presence of three different beads morphologies (Figure 3):

- Unmelted Borders (UB): Only the central portion of the SSTs created a continuous melt pool. In correspondence of the borders, many separated balls were detected. This morphology suggests that the energy density was high enough to melt the deposited powder but that only a very thin layer of molten material was generated. Because of the surface tension, the melt layer collapsed in a thinner scan track and left some residual balls of prior-melt material at the edges of the scanned surface.
- Central Hole (CH): The SSTs appeared overall stable, but some irregularities on the surface were found. These features were mainly detected at the beginning and at the end of track and led to an uneven distribution of the material in the central portion of the bead.

**Table 2** Cubes building parameters. In all cases P = 1500 W, $v_s$ = 600 mm/min

| $d_O$ (mm) | $OV_X$ (%) | dX (mm) | dZ (mm) |
|---|---|---|---|
| 0 | 20 | 2.1 | 0.4 |
| | 30 | 2.4 | |
| | 40 | 3.1 | |
| 0.9 | 20 | 2.4 | 0.4 |
| | 30 | 3.1 | |
| | 40 | 3.8 | |
| 1.7 | 20 | 3.1 | 0.4 |
| | 30 | 3.8 | |
| | 40 | 2 | |
| 2.6 | 20 | 3.8 | 0.4 |
| | 30 | 2 | |
| | 40 | 1.8 | |
| 3.4 | 20 | 2 | 0.5 |
| | 30 | 1.8 | |
| | 40 | 2.1 | |

- Stable and Continuous (SC): These scans were continuous and did not show any relevant defect.

Four different morphologies of the beads were detected by means of cross-section analyses. The morphologies, schematically represented in Fig. 4, are:

- 1 Melt Pool (1MP): A single melt pool, showing the typical shape of the conduction mode bead of non-oscillating DED processes.
- Multiple Melt Pools (MMP): A bead composed of the interconnection of many melt pools whose relative sizes vary, based on the building parameters adopted. The phenomena that might lead to this complex morphology will be discussed later in this paper.
- Flat (Fl): A single melt pool without significant laser penetration in the substrate. As demonstrated by Carrozza et al., this morphology indicates that the energy density is insufficient to melt the substrate [18]. Therefore, the parameters adopted do not seem to be suitable for AM processes, in which the remelting of the previous layer is a key factor for the obtainment of a dense part.
- No Contact (NC): A single drop which has a poor metallurgical bonding with the substrate and results in several areas in which the bead is detached from the baseplate. As in the previous case, this morphology suggests that a low energy density was used. The missing contact between the scan and the substrate suggest that many lack of fusion pores might be generated in an AM process with those parameters [19].

Based on these on-top and cross-sectional classifications of the morphologies, two SSTs process maps were created (Fig. 5). The SSTs represented in the lowest raw of the maps ($d_o$ = 0 mm) are standard DED scans built without deploying the oscillating system. Thus, these are characterised by the conventional morphologies for the DED technology (SC and 1MP). In these cases, the melt pool is formed due to a conduction melting mode and creates a bead showing an appropriate shape, i.e. a good penetration in the substrate and a sufficient growth. The comparison of the SSTs obtained in the other conditions indicates that the SC and CH tracks, which are obtained in the central part of the process window, correspond to the MMP beads. The UB tracks in the on-top analyses (Fig. 3) are associated with the Flat or No Contact melt pools in the cross-section investigation (Fig. 4). These undesired morphologies were detected only when high $d_o$ and low laser power, associated with low scan speeds values, were used. This indicates that the sole ED parameter cannot define the quality of a track. The laser power and the scan speed have to be taken into account separately when an oscillating scanning strategy is used.

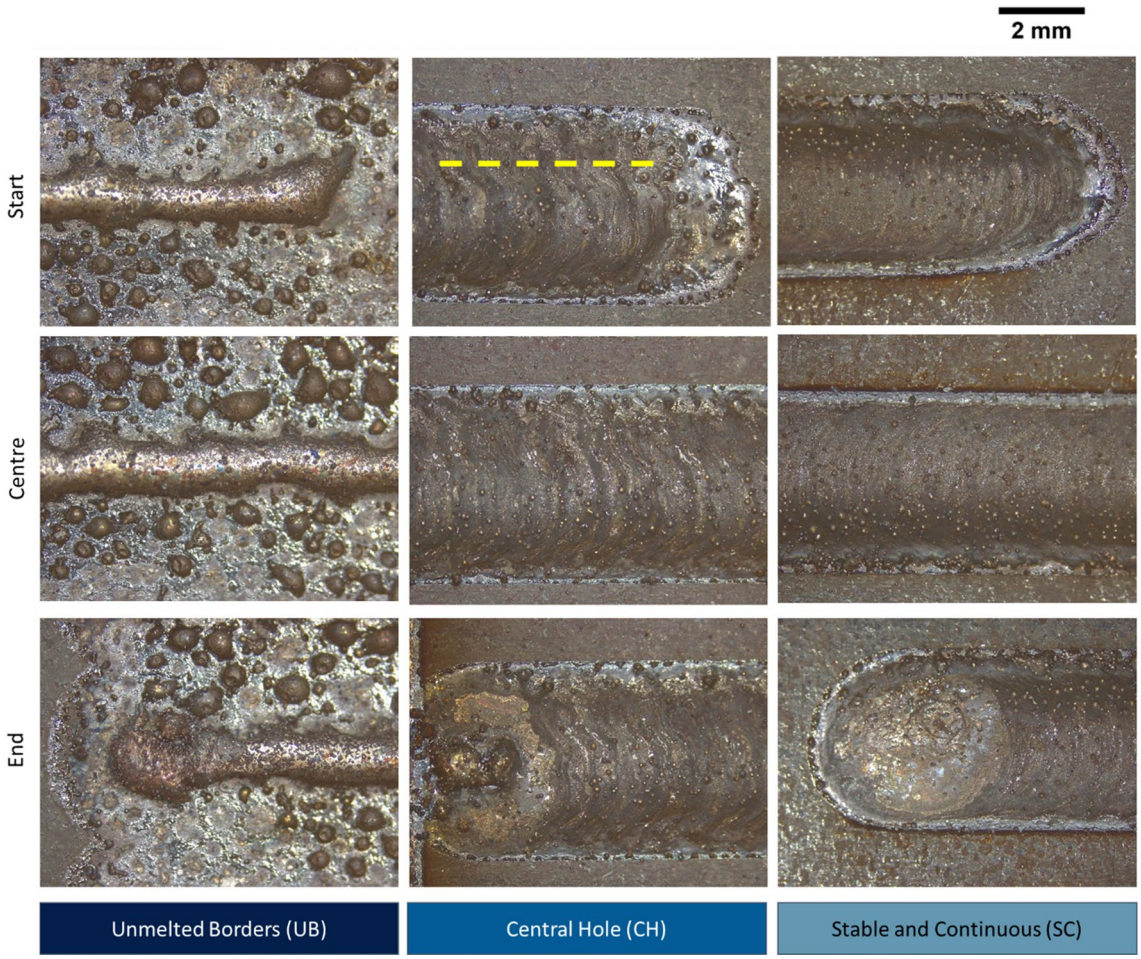


**Fig. 3** Representative on-top micrographs of beads taken at the start, centre and end of the tracks. The yellow line indicates the Central Hole defect

The laser patterns of the four extreme oscillating conditions, reported in Table 3, are represented in Fig. 6, where the laser spot size is represented as well in order to highlight its relative size.

The comparison of the laser patterns and the laser spot indicates that when $d_o$ is larger than $d_F$ (as in set A and set B in Fig. 6) the centre of each circle is not scanned by the laser beam. This might be the reason why in these cases a CH morphology is observed. In all cases, the lateral part of the SSTs patterns appears darker than the central one. This was analysed in more details for the low $d_o$ - low $v_s$ pattern by inspecting more closely the central area and the borders. The comparison of the figures clearly indicates that the laser passes more often in the lateral part of the SSTs. This causes the formation of the multiple melt pools morphologies (Fig. 4 b)).

Once the phenomena occurring in the SSTs were analysed, cubic samples were built using P = 1500 W and v= 600 mm/min. These P and $v_s$ values were selected because, varying $d_o$, they provided all the on-top/cross-sectional morphologies except NC (Fig. 5 b) which, as previously reported, is very unreliable for AM processes. The dX and dZ values calculated according to the melt pools W and G values were evaluated by cross sectional analyses (eq. 3 and 4).

The analyses of the cross-sections of the cubes revealed that in all cases acceptable porosity values (<0.5%) were achieved (Fig. 7a)). These porosity values are in agreement with literature data of 316L DED samples [20, 21]. The reported consolidation values did not show any relevant trend indicating that the detected pores are mainly due to gas porosity not correlated to the used building parameters. The volume of the samples, evaluated with a calliper, is reported in Fig. 7b. All the samples resulted in being slightly larger than the nominal volume which is 8 $cm^3$. All the cubes built with $d_o$=0 mm have very similar volumes close to $V_{th}$. Larger samples are obtained with laser oscillation, resulting in the measured volume values being more scattered. This indicates that, as expected, the laser oscillation reduces the build accuracy of the DED process.

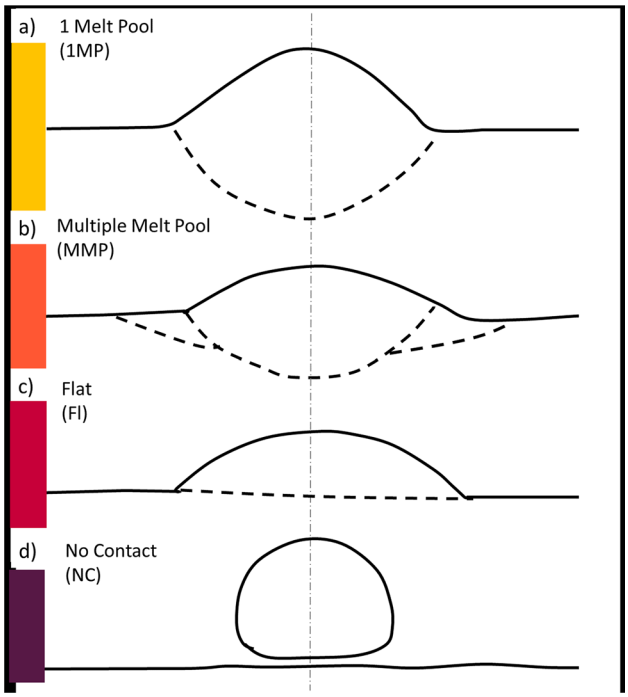


**Fig. 4** Representative images of the SSTs cross-sections: **a** 1 Melt Pool (1MP), **b** Multiple Melt Pools (MMP), **c** Flat (Fl) and **d** No Contact (NC) morphologies

The building rates and the powder efficiencies were then calculated to select the most suitable building conditions (Fig. 7c and d). The comparison of the curves indicates that both BR and η increased with $d_o$ and reached a maximum value when $d_o = 2.6$ mm was used (about + 100% and + 180%, respectively). A $d_o$ value higher than 2.6 mm caused in fact the formation of UB tracks having a reduced width with respect to the laser pattern due to the collapse of the thin molten layer. These low melt pool width values cause low dX displacement values (Eq. 3). Because of the low distance among nearby tracks, a large number of tracks per layer are needed. Figure 7d also includes a comparison with a BR value calculated from the parameters of traditional DED depositions having similar set-ups to the ones here adopted [22]. It is important to underline that among the process parameters, the dX and dZ are the most impacting factors concerning the BR and that DED process of stainless steels can theoretically be obtained with dX and dZ in the range 0.2–1.3 mm. This leads to a very large range of BR values available in the literature ($\left(10 \div 150\ \mathrm{cm}^3/h\right)$ [22, 23]. Even if the powder efficiency aspect plays a key-role in the industrial application of the DED process as it directly influences the process costs, it is not very discussed in the literature. Only a few papers, in fact, reported the efficiency data (ranging from 5 to 70%) and stated these values are strongly dependant on the nozzle configuration and on the building parameters [24].

To sum up, the results reported in Fig. 7 indicate that dense 316L samples can be obtained with all the building parameters tested in this work and that the highest build rate and powder efficiency can be obtained with a $d_o$ value of 2.6 mm. These parameters result however in a lower geometrical accuracy than the $d_o$=0 mm condition.

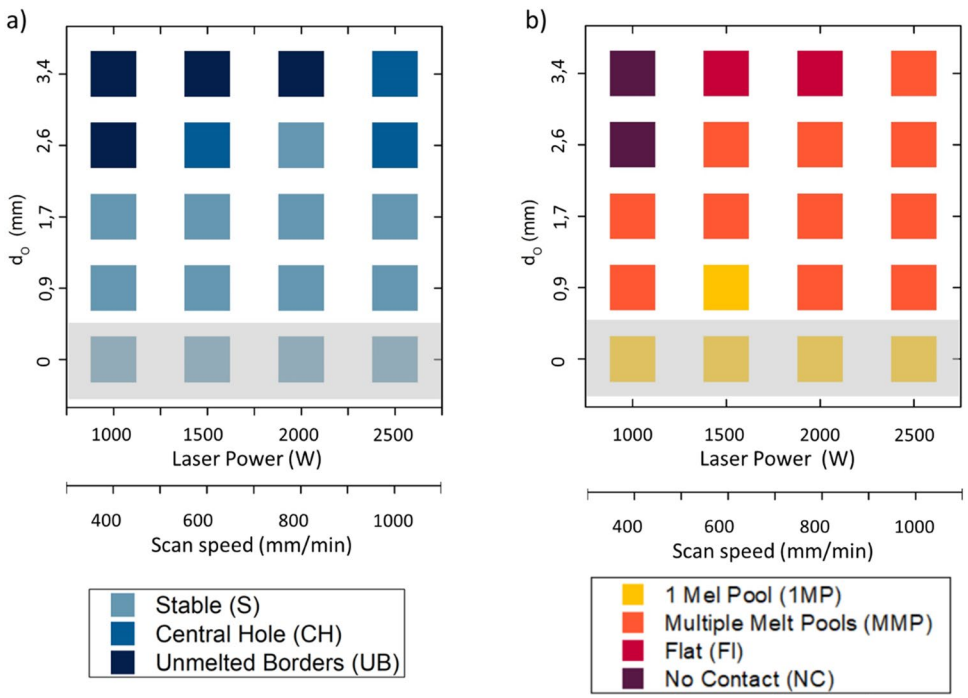


**Fig. 5** Process maps of SSTs evaluated by **a** on-top and **b** cross-section. The grey areas indicate the non-oscillating conditions

**Table 3** SSTs parameters whose patterns are represented in Fig. 6

| | P (W) | $v_s$ (mm/min) | $d_o$ (mm) |
|---|---|---|---|
| Set A | 2500 | 1000 | 3.4 |
| Set B | 1000 | 400 | 3.4 |
| Set C | 2500 | 1000 | 0.9 |
| Set D | 1000 | 400 | 0.9 |

The microstructure of DED samples built with different $d_o$ and $OV_X$ values are reported in Fig. 8. Some spherical micrometric dark particles can be detected in all the samples. These particles can be Mn, Si oxides which are quite common in AM of 316L parts [25]. A closer look to the images reveals that the oxide dimension increases with the oscillation. The reason of the different size might be the different oxidation kinetic due to the decrease of the laser intensity $I_L = P/d$ (where d is the apparent laser spot). The $d_o$ increase causes the enlargement of the area impinged by the laser, thus a higher melt-pool residence time [26].

From a microstructural point of view, all the samples are characterised by a fine dendritic microstructure made of γ-cells and some δ-ferrite. It is well known that the size and the morphology of the dendrites depend on the cooling conditions such as the thermal gradient at the liquid/solid interface (G), and the solidification rate (R). The larger size of the dendrites obtained using large $d_o$ values (Fig. 8b and d) confirms that the oscillating strategy involves lower solidification rates with respect to the standard DED process. A quantitative representation of this phenomenon can be extracted from the average Primary Dendrite Arm Spacing (values reported in Fig. 8). According to Guo et al. the relationship between average PDAS and cooling rate ($\dot{T}$) provide a clear overview on the thermal history undergone by the part [27].

$$PDAS = 80\dot{T}^{-0.33} \tag{7}$$

Moreover, a closer look at the micrographs, denotes that the content of δ-ferrite changes due to the DED parameters. It is well established that the ferrite content can be estimated based on the steel composition using the Schaeffler or WRC-1992 diagrams. However, these diagrams do not consider the effect that the solidification rate has on the ferrite content. According to the Pseudo-binary phase diagram, steels that have a low $Cr_{eq}/Ni_{eq}$ ratio (<1.6), such as 316L, solidify in the austenite (A) or primary-austenite with second-phase ferrite (AF) modes. As described by Elmer et al., for these compositions, the ferrite content decreases as the cooling rate increases because less original ferrite forms [28]. This result also confirms that the samples built with the oscillating strategy solidify with a

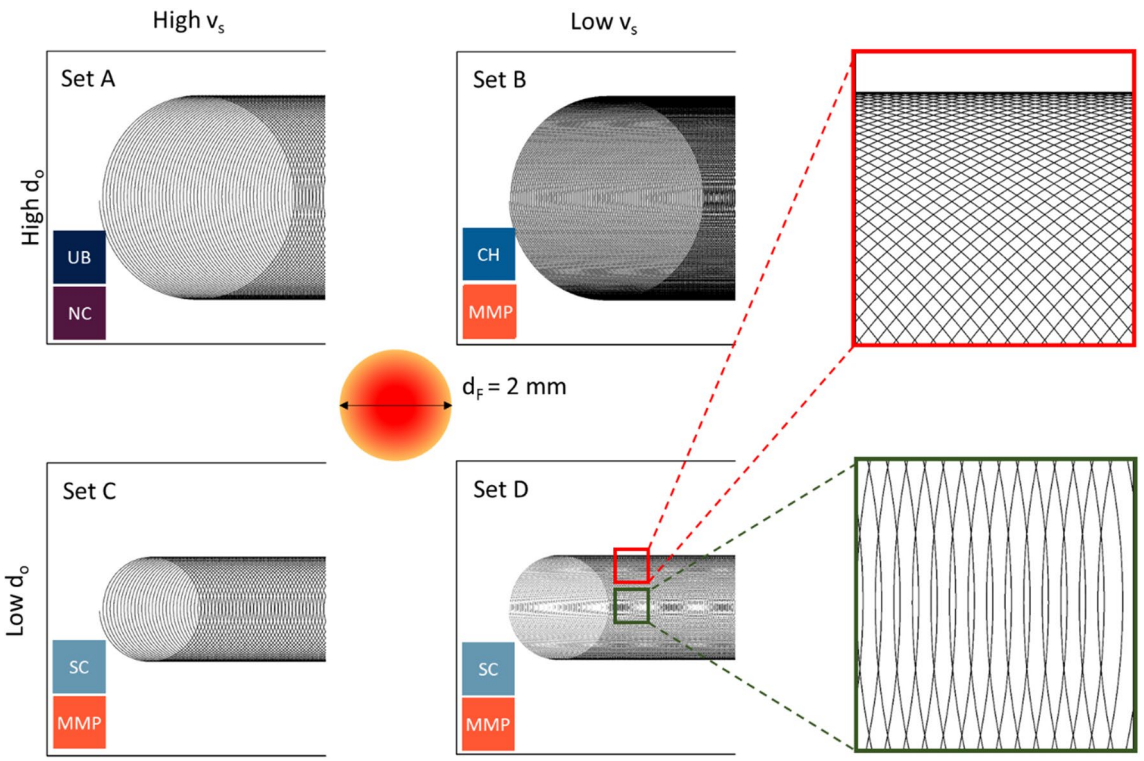


**Fig. 6** Schematic representation of the laser patterns of the sets reported in Table 3. The red spot in the centre represents the nominal laser spot (2 mm)

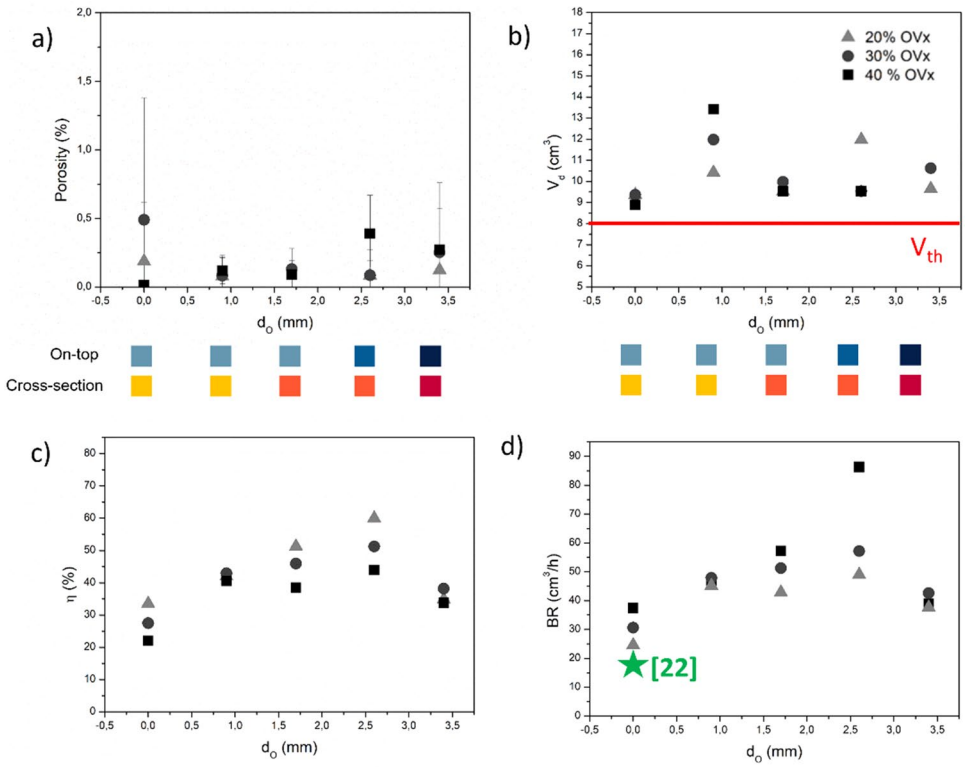


**Fig. 7** **a** Porosity, **b** deposited Volume ($V_d$), **c** Powder efficiency (η) and **d** Building rate (BR) VS oscillating diameter. The colours reported underneath the graphs indicate the on-top and cross-section morphologies of the SSTs. The BR value from [22] was calculated according to the scan speed, dX and dZ values of a DED systems having similar settings

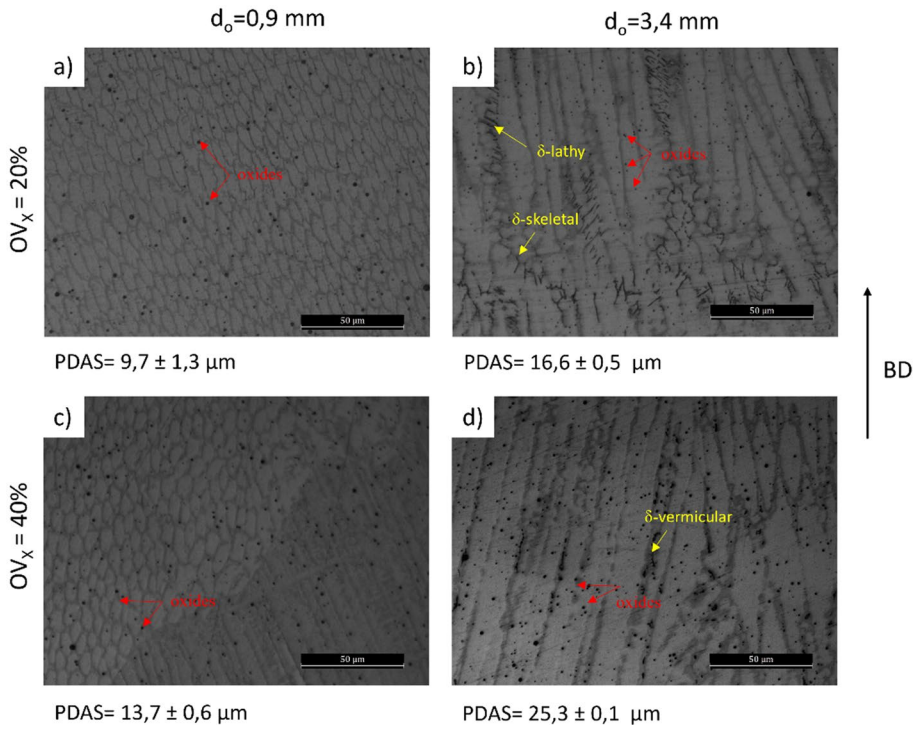


**Fig. 8** Optical micrographs of 316L DED samples built with **a** and **c** $d_o$ = 0.9 mm, **b** and **d** $d_o$ = 2.6 mm. **a** and **b** with OVx = 20% and **c** and **d** with OVx = 40%. The black arrow indicates the building direction (BD)

lower cooling rate with respect to the non-oscillating one. Finally, different ferrite morphologies (lathy or skeletal) were detected in the samples. As reported in the literature, the different morphologies are related to the ferrite content [29, 30].

The effect of the oscillation diameter on the mechanical behaviour was analysed by Vickers hardness tests. The

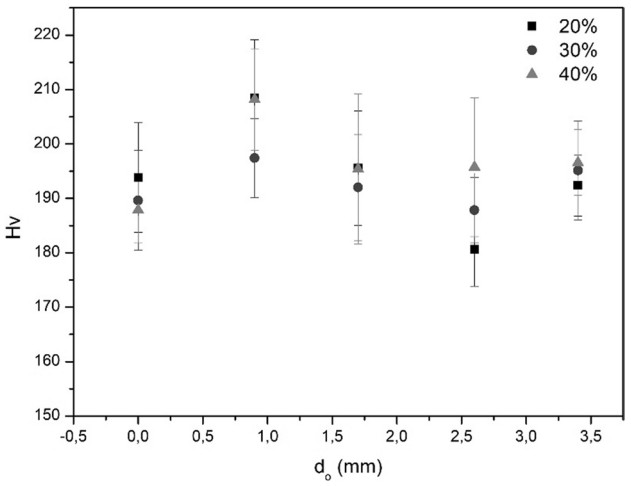


**Fig. 9** Hardness VS $d_o$ trends for each overlap

results, reported in Fig. 9, indicate that there is only a slight correlation between the $d_o$ value and the hardness. This correlation is however not very relevant if the standard deviation values are considered. Based on the microstructural results, the consequence of the oscillation on hardness could be quite complex due to the synergic effect of the δ-ferrite content and the cells size (Fig. 8). On the one hand, in fact, the high δ-ferrite content of the high $d_o$ samples, causes an increase in hardness. On the other hand, the larger cells present in samples produced with high oscillation values causes a decrease in hardness.

Finally, the effect of the oscillating parameters on the surface quality of the specimens was analysed by means of confocal imaging (Fig. 9 and Table 4). The surface scans (Fig. 10) highlighted that the surface quality was mostly determined by the visible layers. In fact, the highest points of the surfaces clearly corresponded to the centres of every layer. The only notable exception was the sample built using $d_o$ = 2.6 mm and $OV_X$ = 40%. In this case, vertical tracks, up to 2.5 mm height, were detected throughout the whole surface. This effect might be the result of an overabundance of molten material deposited, which then reaches the outer edge on the material. The roughness data of the samples' lateral surfaces, reported in Table 4, indicate that the samples built with lower oscillations ($d_o$ =0.9 mm) are characterised by lower roughness (Sa) and waviness (Sz) than those built with the highest oscillating strategy ($d_o$=3.4 mm). The highest roughness was detected when high oscillation is associated to a high X overlap. Correlations between the building parameters and roughness values have been also previously reported in the literature [31, 32]

## 4 Conclusions

This work evaluated the applicability of the oscillating scanning strategy to the DED process with the aim of rapidly modifying the powder efficiency and the building rate. In the first experimental step, the effect of the main DED oscillating parameters (e.g. P, $v_s$ and $d_o$) on the morphologies and stabilities of the SSTs was assessed by on-top and cross-section analyses. The study of the beads revealed 3 on-top and 4 cross-sectional types of morphologies. In order to understand the phenomena that arise during laser scanning, process maps were designed based on the on-top and cross-sectional morphologies. By the comparison of these maps, the phenomena that lead to each specific morphology were understood:

- When $d_o$ = 0 mm, the oscillating strategy is not used and therefore a standard DED process takes place. Tracks obtained with $d_o$ = 0 mm are characterised by a stable morphology and a single melt pool (1MP). As the P and $v_s$ values used in this study are suitable for the DED process of this alloy, the melt pool is created in a conduction melting mode and the bead is characterised by an appropriate geometry.
- When low P and low $v_s$ are associated with high $d_o$, unstable scan tracks with poor penetration in the substrate are formed. By means of on-top analyses, a thin scan track surrounded by many separated balls can be detected, thus indicating that the energy density was sufficient to create a thin layer of molten material, but insufficient to penetrate in the substrate. During cooling, because of the surface tension, this thin layer collapses in a central thin track and fine balls. This hypothesis is confirmed by the cross-sectional analyses that revealed a poor penetration of the bead in the substrate associated to this on-top morphologies.
- In the remaining conditions (i.e. low $d_o$ associated with low P and $v_s$ or all the $d_o$ combined to high P and $v_s$), mainly stable scan tracks are formed. The scan track

**Table 4** Roughness and waviness values of samples built with different parameters

| $d_o$ (mm) | OVx (%) | Sa (μm) | Sz (μm) |
|---|---|---|---|
| 0.9 | 20 | 55 | 662 |
| 3.4 | 20 | 83 | 1097 |
| 0.9 | 40 | 63 | 721 |
| 3.4 | 40 | 287 | 2108 |

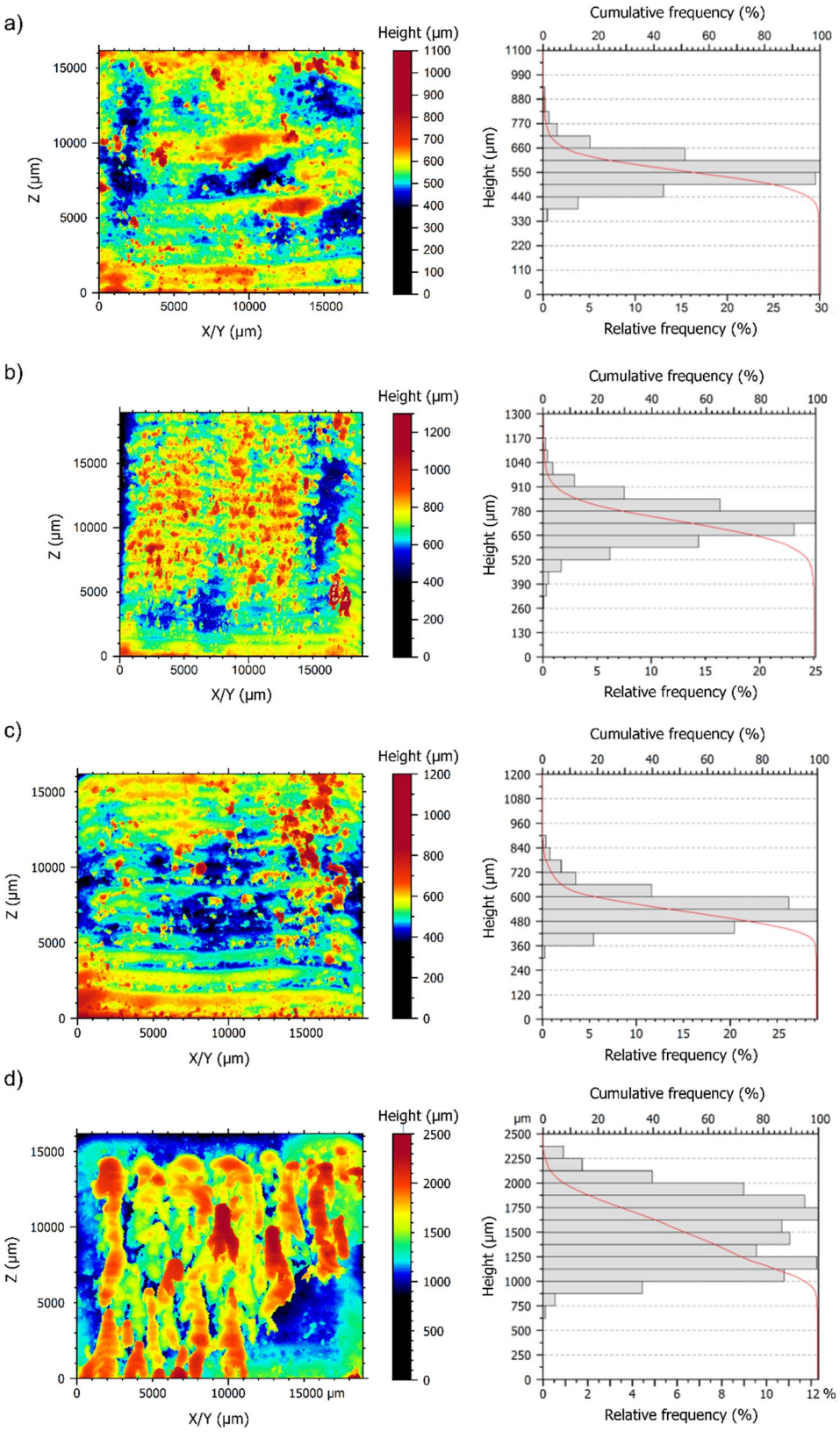


**Fig. 10** Surface scans and relative height distribution curves of the 316L DED-processed samples built with **a** and **c** $d_o = 0.9$ mm, **b** and **d** $d_o = 2.6$ mm. **a** and **b** with OVx = 20% and **c** and **d** with OVx = 40% X

built with these parameters result being continuous and do not show any relevant defect in both, the on-top and cross-section analyses.

In the second experimental step, 316L cubes were built using some of the SSTs investigated parameters and three X overlap values. The outcomes of the cube analyses can be summarised as follows:

- The cubes porosity values indicated that it is possible to obtain dense samples with all the oscillating diameters if the correct track overlaps are used. The obtained building rate and powder efficiency values confirmed that the oscillating strategy can improve the overall performances of the DED process (about + 100% and + 180% respectively).
- The microstructures of all the samples display the different cooling rate that the material experienced due to the different oscillating parameters. The samples with high $d_o$ are in fact characterised by larger dendrites and higher ferrite content with skeletal or lathy morphologies.
- The samples built with the oscillating strategy had scattered volume values always larger than the nominal one. This indicates that, as expected, the large apparent laser spot reduces the build accuracy of DED. The surface analyses also confirm that high oscillating diameters reduce the quality of the part surfaces.

Therefore, all of the building condition evaluated in the present study could be suitable to produce dense 316L samples and the authors suggest to select the oscillating diameter based on the build rate and geometrical accuracy requirements. The main advantage of this deposition strategy is related to the possibility of effectively varying the oscillating parameter within a single part. The effect of the use of different parameters in a single component will be investigated in future works.

**Acknowledgements** The authors would like to acknowledge Dr. Erica Librera from Prima Additive (a division of Prima Industrie S.p.A.) for the production of samples and for her support in the experimental activities. The authors would like also to appreciate the assistance provided by Simone Bleynat, Andrea Pastorino and Nicola Ripoli in data analyses.

## Declarations

**Conflict of interest** On behalf of all authors, the corresponding author states that there is no conflict of interest.



## References

1. M.H. Farshidianfar, A. Khajepour, A.P. Gerlich, J. Mater. Process. Tech. **231**, 468–478 (2016). https://doi.org/10.1016/j.jmatprotec.2016.01.017
2. A. Saboori, S. Biamino, M. Lombardi, S. Tusacciu, M. Busatto, M. Lai, P. Fino, Powder Metall. **62**, 213–217 (2019). https://doi.org/10.1080/00325899.2019.1627490
3. Z. Francis, The Effects of Laser and Electron Beam Spot Size in Additive Manufacturing Processes, Ph.D. Dissertation, Carnegie Mellon University (2017). https://search.proquest.com/docview/1906683857?fromunauthdoc=true&pq-origsite=gscholar%0Ahttp://repository.cmu.edu/dissertations/909.
4. R.P. Mudge, N.R. Wald, Weld. J. **86**, 44–48 (2007)
5. Z. Wang, T.A. Palmer, A.M. Beese, Acta Mater. **110**, 226–235 (2016). https://doi.org/10.1016/j.actamat.2016.03.019
6. B. Li, B. Wang, G. Zhu, L. Zhang, B. Lu, Materials **14**, 4265 (2021). https://doi.org/10.3390/ma14154265
7. D. Miller, C. Deckard, J. Williams, Rapid Prototyp. J. **3**, 4–11 (1997). https://doi.org/10.1108/13552549710169237
8. C. Yi, L. Dichen, W. Jing, Rapid Prototyp. J. **19**, 100–110 (2013). https://doi.org/10.1108/13552541311302950
9. A. Müller, S.F. Goecke, M. Rethmeier, Weld. World. **62**, 1039–1047 (2018). https://doi.org/10.1007/s40194-018-0625-3
10. L.H. Shah, F. Khodabakhshi, A. Gerlich, J. Manuf. Process. **37**, 212–219 (2019). https://doi.org/10.1016/j.jmapro.2018.11.028
11. S.V. Kuryntsev, A. Kh. Gilmutdinov, Int. J. Adv. Manuf. Technol. **81**, 1683–1691 (2015). https://doi.org/10.1007/s00170-015-7312-y
12. H. Ramiarison, N. Barka, C. Pilcher, E. Stiles, G. Larrimore, S. Amira, J. Laser Appl. **33**, 032015 (2021). https://doi.org/10.2351/7.0000353
13. C. Hagenlocher, M. Sommer, F. Fetzer, R. Weber, T. Graf, Mater. Design **160**, 1178–1185 (2018). https://doi.org/10.1016/j.matdes.2018.11.009
14. S.W. Bae, J.S. Kim, D.S. Kim, S.Y. Yoo, An experimental study for rising manufacturing time and accuracy on SLS process, in *2009 IEEE International Symposium on Assembly and Manufacturing*. Seoul, 17-20 November 2009 (IEEE, Piscataway, 2009), pp. 83–87. https://doi.org/10.1109/ISAM.2009.5376924
15. A. Saboori, A. Aversa, F. Bosio, E. Bassini, E. Librera, M. de Chirico, S. Biamino, D. Ugues, P. Fino, M. Lombardi, Mater. Sci. Eng. A **766**, 138360 (2019). https://doi.org/10.1016/j.msea.2019.138360
16. A. Aversa, G. Marchese, E. Bassini, Metals **11**, 932 (2021). https://doi.org/10.3390/met11060932
17. D.F. Franco, Wobbling laser beam welding of copper, Dissertation, FCT NOVA - Universidade NOVA de Lisboa (2017). http://hdl.handle.net/10362/27684
18. A. Carrozza, F. Mazzucato, A. Aversa, M. Lombardi, F. Bondioli, S. Biamino, A. Valente, P. Fino, Met. Mater. Int. **27**, 3590–3602 (2021). https://doi.org/10.1007/s12540-020-00930-3
19. N.T. Aboulkhair, I. Maskery, C. Tuck, I. Ashcroft, N.M. Everitt, J. Mater. Process. Tech. **230**, 88–98 (2016). https://doi.org/10.1016/j.jmatprotec.2015.11.016
20. Z.E. Tan, J.H.L. Pang, J. Kaminski, H. Pepin, Addit. Manuf. **25**, 286–296 (2019). https://doi.org/10.1016/j.addma.2018.11.014

21. B. Zheng, J.C. Haley, N. Yang, J. Yee, K.W. Terrassa, Y. Zhou, E.J. Lavernia, J.M. Schoenung, Mater. Sci. Eng. A **764**, 138243 (2019). https://doi.org/10.1016/j.msea.2019.138243
22. Z. Li, S. Sui, X. Ma, H. Tan, C. Zhong, G. Bi, A.T. Clare, A. Gasser, J. Chen, Int. J. Mach. Tools Manuf. **181**, 103942 (2022). https://doi.org/10.1016/j.ijmachtools.2022.103942
23. D.-G. Ahn, Int. J. Precis. Eng. Manuf. Green Tech. **8**, 703–742 (2021). https://doi.org/10.1007/s40684-020-00302-7
24. K.L. Terrassa, J.C. Haley, B.E. MacDonald, J.M. Schoenung, Powder Technol. **338**, 819–829 (2018). https://doi.org/10.1016/j.powtec.2018.07.065
25. A. Aversa, A. Saboori, E. Librera, M. de Chirico, S. Biamino, M. Lombardi, P. Fino, Addit. Manuf. **34**, 101274 (2020). https://doi.org/10.1016/j.addma.2020.101274
26. D.-R. Eo, S.-H. Park, J.-W. Cho, Addit. Manuf. **33**, 101119 (2020). https://doi.org/10.1016/j.addma.2020.101119
27. D. Guo, K. Yan, M.D. Callaghan, D. Daisenberger, M. Chatterton, J. Chen, A. Wisbey, W. Mirihanage, Mater. Design **207**, 109782 (2021). https://doi.org/10.1016/j.matdes.2021.109782
28. J.W. Elmer, S.M. Allen, T.W. Eagar, The influence of cooling rate on the ferrite content of stainless steel alloys, in *Proceedings of the 2nd International Conference on Trends in Welding Research, TWR '89*. Gatlinburg, 14-18 May 1989 (ASM International, Materials Park, 1990), pp. 165–170
29. T. Takalo, N. Suutala, T. Moisio, Metall. Trans. A **7**, 1591–1592 (1976). https://doi.org/10.1007/BF02656405
30. E.M.F. de Souza Silva, G.S. da Fonseca, E.A. Ferreira, J. Mater. Res. Technol. **15**, 4317–4329 (2021). https://doi.org/10.1016/j.jmrt.2021.10.009
31. K.S.B. Ribeiro, F.E. Mariani, R.T. Coelho, Procedia Manuf. **48**, 663–670 (2020). https://doi.org/10.1016/j.promfg.2020.05.158
32. A. Ascari, A.H.A. Lutey, E. Liverani, A. Fortunato, Lasers Manuf. Mater. Process. **7**, 426–448 (2020). https://doi.org/10.1007/s40516-020-00128-w